minerals

MDPI

Article

Influence of Liquid CO_2 Extraction and Dissolution on Coal Adsorption Characteristics

Hu Wang [1,*], Hu Wen [2], Zhenbao Li [1,*] and Wansheng Mi [2]

[1] College of Petroleum and Chemical Engineering, Lanzhou University of Technology, Lanzhou 730050, China
[2] College of Safety Science and Engineering, Xi'an University of Science and Technology, Xi'an 710054, China; 19120089013@stu.xust.edu.cn (H.W.); lih@163.com (W.M.)
* Correspondence: wanghu@lut.edu.cn (H.W.); lizb@lut.edu.cn (Z.L.)

Abstract: Liquid CO_2 is a non-polar fluid, and the injection of CO_2 fluid into a coal seam causes a strong water–rock interaction between the inorganic minerals and organic matter in the coal and acidic fluid. The minerals in the coal are thereby corroded and precipitated to different degrees, and the organic matter is dissolved and extracted, which further changes the physical and chemical properties of the coal and rock. Three kinds of coal samples with different metamorphic degrees were selected as the research objects, and the research methods of theoretical analysis and experimental testing were used to carry out the related research on the modification of coal by liquid CO_2 extraction and dissolution. After the three kinds of coal samples were extracted by liquid CO_2, the pore specific surface area decreased and the CO_2 adsorption decreased with the increase in extraction pressure. The reduction in anthracite adsorption was greater than that of bituminous coal and lignite; after being corroded by different CO_2 pressures, the adsorption capacity of bituminous coal gradually increased with the increase in corrosion pressure, and the increase in adsorption capacity of bituminous coal was larger than that of anthracite and lignite. After corrosion, bituminous coal was suitable for CO_2 geological storage.

Keywords: low permeability; liquid CO_2; extraction; dissolution; adsorption

Citation: Wang, H.; Wen, H.; Li, Z.; Mi, W. Influence of Liquid CO_2 Extraction and Dissolution on Coal Adsorption Characteristics. *Minerals* **2023**, *13*, 650. https://doi.org/10.3390/min13050650

Academic Editor: Tuncel M. Yegulalp

Received: 4 April 2023
Revised: 5 May 2023
Accepted: 7 May 2023
Published: 8 May 2023

1. Introduction

Mine gas, also known as coalbed methane, serves as not only a primary hazard endangering coal mine safety but also an efficient, green, and clean unconventional natural gas resource [1,2]. Gas extraction is the most effective method for eliminating gas-related disasters. Actively implementing enhanced gas extraction not only ameliorates coal mine safety [3–5], but also aids in obtaining clean energy, augmenting mine economic benefits, diminishing carbon emissions, and preserving the atmospheric environment. Over 50% of the more than 11,000 mines in China are high-gas or coal and gas outburst mines, with most high-gas coal seams being low permeability seams, exhibiting coal seam permeability between (0.001~0.1) $\times 10^{-3}$ D and low average air permeability [6–8]. Coal seam permeability, a macroscopic parameter representing pore and fracture development in coal, differs due to variations in pore and fracture width, length, and density, leading to fluid flow and fracture propagation discrepancies during liquid CO_2 injection and, ultimately, affecting seam stimulation [9]. Traditional coal seam permeability is categorized into low, medium, and high permeability, based on thresholds of $<0.1 \times 10^{-3}$ D, $(0.1\sim1.0) \times 10^{-3}$ D, and $>1.0 \times 10^{-3}$ D, respectively. However, permeability in most Chinese coal seams is below 0.1×10^{-3} D, classifying them as low-permeability coal seams [10–15]. As mining depth increases, coal seam permeability declines, necessitating the innovation of efficient permeability enhancement technologies for coal seams and the improvement of gas extraction efficacy [16].

The predominant mechanism of gas adsorption in coal is physical adsorption. With the increasing implementation and application of CO_2-ECBM (CO_2-enhanced coal bed

methane), research on the competitive adsorption and desorption of CO_2/CH_4 in coal has gradually progressed. Kross performed CO_2 and CH_4 adsorption experiments at 20 Mpa pressure with varying metamorphic degrees [17]; Stevenson conducted experiments on CH_4 and CO_2 mixed gas adsorption by coal [18]; Greaves determined that hysteresis exists between adsorption isotherms and desorption isotherms under adsorption phase experimental conditions [13]; Abunowara investigated CO_2 adsorption utilizing adsorption isotherm, thermodynamic, and kinetic models, revealing that CO_2 adsorption on coal is random and pore diffusion primarily controls the CO_2 adsorption process in coal matrices [19]; Shang demonstrated that adjusting the parameters of liquid CO_2 phase change blasting reduces coal and gas outburst risks in coal seams [20]; Li discovered that after liquid CO_2 saturation, the amount of CO_2 filling coal micropores diminished [21]; and Zhai concluded that altering the nozzle diameter had a more significant effect on the cooling range than changing the liquid CO_2 mass flow rate [22].

Coal seams, comprising matrix pores and natural fracture networks, are anisotropic mediums where internal pore and fracture structure characteristics govern gas storage and migration. Following liquid CO_2 extraction and dissolution, coal's pore structure characteristics undergo alterations, thereby affecting CO_2 adsorption and diffusion properties within the coal. This study, grounded in CO_2 adsorption experiments, compares and analyzes experimental data from raw and residual coal to investigate the variation of related parameters during the diffusion processes of both raw and residual coal.

2. CO_2 Adsorption Theory

At constant temperature with varying pressure, the adsorption process of CO_2 in coal is isothermal, and the adsorption isotherm type mainly depends on the adsorbent and adsorbate participating in the reaction. Distinct solid and gas combinations result in different adsorption isotherm trends. Figure 1 illustrates the types of gas adsorption isotherms on solid surfaces.

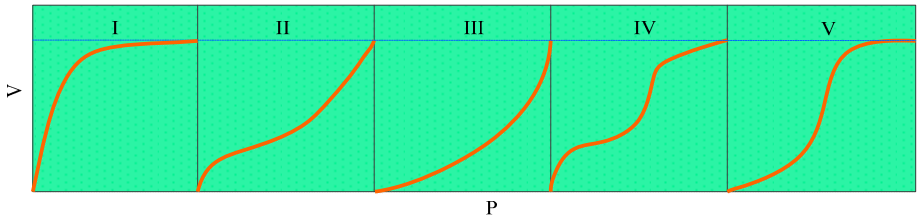

Figure 1. Types of gas adsorption isotherms on solid surfaces.

In coal CO_2 adsorption, there is no separation between adsorption and desorption molecules. When the adsorbent contains 2.0 to 3.0 nm micropores, multilayer adsorption and capillary condensation occur; however, the isothermal adsorption curve remains Type I. Micropores fill with adsorbate molecules, while macropores typically experience multilayer adsorption. At room temperature, coal primarily adsorbs CO_2 gas molecules in micropores, as depicted in the micropore filling adsorption model in Figure 2.

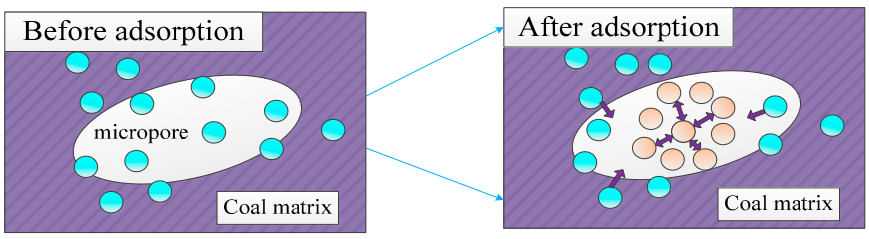

Figure 2. Micropore filling adsorption model.

Three prevalent adsorption models employed to examine coal adsorption gas include the Langmuir adsorption model, the Dubinin-Astakhov (D–A) adsorption model, and the

Brunauer–Emmett–Teller (BET) adsorption model. The adsorption isotherm between coal and CO_2 is consistent with the Type I adsorption isotherm, rendering the Langmuir and BET adsorption models appropriate for examining this isotherm type. Consequently, this section utilizes the Langmuir and BET models for fitting. Figure 3 presents schematic representations of the Langmuir monolayer adsorption model and the BET multilayer adsorption model.

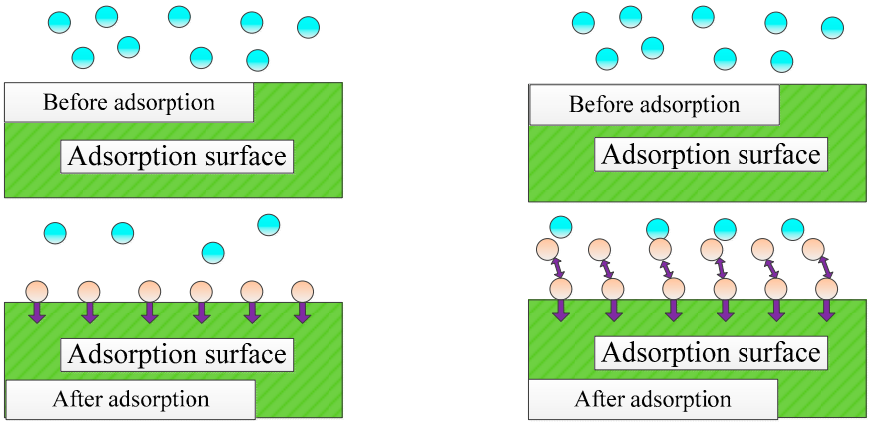

Figure 3. Langmuir monolayer adsorption model and BET multilayer adsorption model.

The Langmuir adsorption model postulates that a single atom or molecule can be adsorbed at each site on a solid surface, exemplifying ideal monolayer adsorption. Under the assumption of an unsaturated atomic force field and uniform adsorption capacity across the solid surface, the dynamic adsorption equilibrium can be represented by the following formula:

θ denotes the adsorbate coverage percentage, which is expressed as:

$$\theta = \frac{S_\theta}{S_t} \tag{1}$$

where θ is the adsorption mass coverage, %; S_θ is the surface area of the solid covered by adsorbate (m^2), and S_t is the total surface area of the solid (m^2).

Upon reaching equilibrium, the adsorption rate equals the desorption rate. As per gas molecule motion theory, the number of collision molecules (N) per unit surface area and time is:

$$N = \frac{P}{\sqrt{2\pi mkT}} \tag{2}$$

where N is the number of collision molecules per unit surface area per unit time, P is the gas pressure (MPa), m is the molecular mass of gas (g), k is the Boltzman constant, and T is the absolute temperature (K).

The fraction adsorbed in the collision molecule is symbolized by α. In accordance with the Langmuir model's basic assumptions, the adsorption rate (V_a) and desorption rate (V_d) are expressed as:

$$V_a = \alpha N(1-\theta) \tag{3}$$

$$V_d = v\theta \tag{4}$$

where, V_a and V_d are adsorption rates and desorption rates, respectively (cm^3/s), α is the fraction adsorbed in the collision molecule, and v is the desorption proportional constant, which is the desorption rate when $\theta = 1$.

When the adsorption reaches equilibrium, $V_a = V_d$, and Langmuir isotherm is expressed as:

$$Q = \frac{abP}{1+bP} \tag{5}$$

where a and b are adsorption equilibrium constants.

The Langmuir adsorption model, based on the premise of single-molecule adsorption at each site on a solid surface, is insufficient for describing multilayer adsorption behavior. Consequently, the BET (Brunauer, Emmett, and Teller) adsorption model has been developed to address this limitation by extending the monolayer adsorption theory to encompass multilayer adsorption. The BET adsorption model's calculation formula is as follows:

$$Q = \frac{V_m}{P_0 - P}\left[\frac{1-(d+1)(P/P_0)^d + n(P/P_0)^{d+1}}{1-(C-1)(P/P_0)^d + C(P/P_0)^{d+1}}\right] \quad (6)$$

where P_0 is the saturated vapor pressure of adsorbate at a fixed temperature (MPa), C is the heat of liquefaction between adsorbent and adsorbate in the adsorption process is a fixed constant, V_m represents the saturated adsorption capacity of the first layer (cm^3/g), and d is a fixed constant, which is related to temperature, pore distribution, etc.

3. Experimental System and Process

3.1. Experimental System

The self-constructed experimental platform for liquid CO_2 extraction and dissolution comprises components such as a CO_2 cylinder, booster pump, vacuum pump, reaction kettle, collection and analysis system, and data acquisition system. The schematic diagram of the experimental equipment is presented in Figure 4.

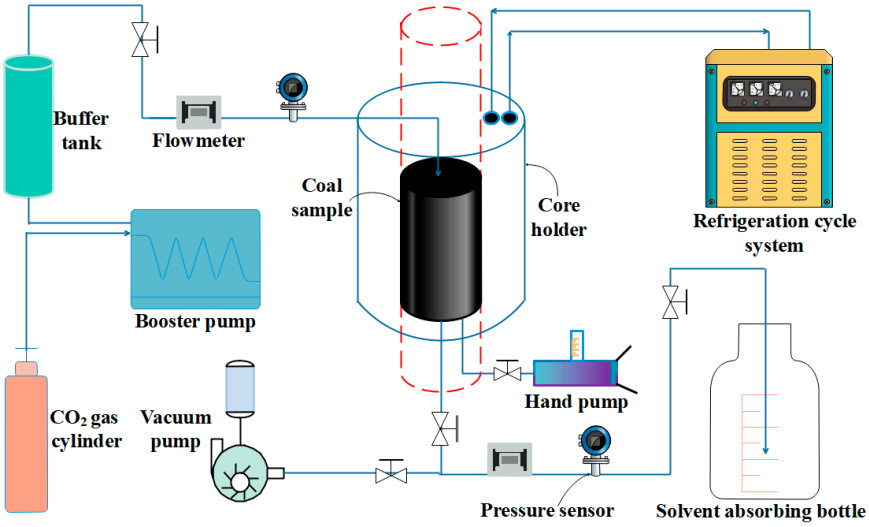

Figure 4. Schematic diagram of liquid CO_2 extraction and dissolution experiment system.

The experimental procedure involved collecting fresh coal samples and processing them into Φ50 × 100 cylindrical specimens. In the extraction experiment, coal samples were dried, and liquid CO_2 was introduced into the reaction kettle via the booster pump. The outlet valve was opened, permitting liquid CO_2 to dynamically extract organic matter from the coal. In the dissolution experiment, the outlet valve was closed, and a coal sample saturated with water was sealed in the reactor. CO_2 was then introduced into the reactor to facilitate a complete reaction.

The experimental apparatus utilized a custom-designed CO_2 adsorption system, which primarily consists of a gas supply system, a high-temperature and pressure closed container, a temperature control system, a vacuum pumping system, and a data acquisition system. The experimental schematic and physical diagrams are presented in Figure 5.

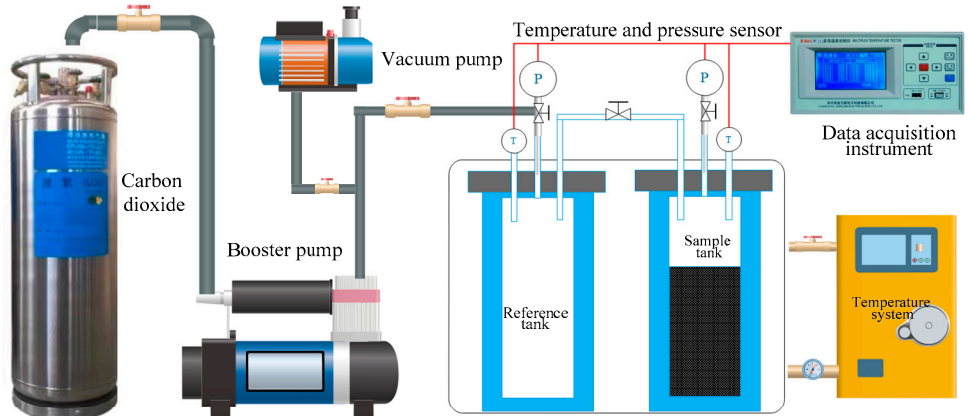

Figure 5. Schematic diagram of CO_2 adsorption experiment system.

The gas supply system comprised a CO_2 gas cylinder, pressure regulator, three-way valve, and other components. The pipeline was constructed from 3 mm stainless steel high-pressure tubing. The high-temperature reaction vessel was fabricated from stainless steel, with pressure and temperature ranges of 0 to 50 MPa and −30 to 150 °C, respectively. The vacuum system consisted of a vacuum pump, valve, and pipeline, with a pumping rate of 1.5 CFM and an ultimate vacuum pressure of 5 Pa. The data acquisition system included a temperature sensor, gas pressure sensor, and signal converter. The gas pressure sensing range was 0 to 10 MPa, with an accuracy of 0.0001, and the signal converter was a DAQM-4206 signal converter.

3.2. Experimental Principle and Process

The experiment was based on the ideal gas equation of state:

$$PV = nZRT \tag{7}$$

where V is the gas volume (cm^3), n is the amount of substance (mol), Z is the gas compression factor (dimensionless), and R is the gas constant, 8.314 J/(mol·K).

The relationship curve between the CO_2 compression factor and pressure is shown in Figure 6.

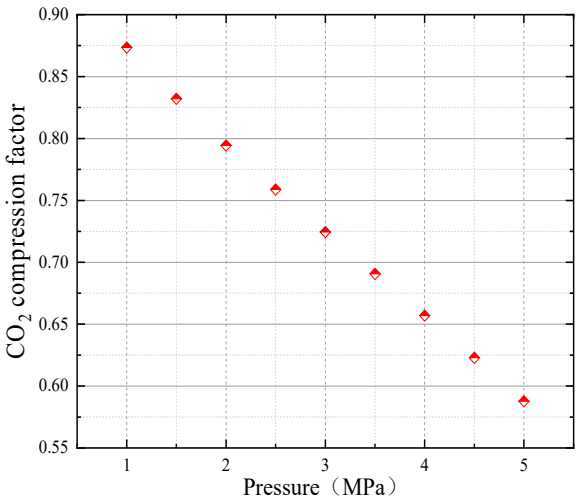

Figure 6. CO_2 gas compression factor and pressure relationship curve.

4. Experimental Results and Analysis

4.1. CO_2 Adsorption Characteristics before and after Coal Extraction

Various factors influence the adsorption of CO_2 by coal. While the fundamental characteristics of coal (such as pore structure) dictate the adsorption behavior in a specific environment, alterations in the physical and chemical environments can still impact the coal's adsorption capacity. During CO_2-ECBM, it takes time for CO_2 to reach adsorption equilibrium. The adsorption equilibrium time for coal and rock is closely related to the diffusion coefficient; the larger the coefficient, the shorter the time required to achieve equilibrium. This study designed the adsorption experiment pressure to range from 0 to 5 MPa and maintained a constant temperature of 25 °C. The isothermal adsorption curves for three dry coal samples in a constant temperature environment are depicted in the following figure.

The adsorption Isotherms for raw and residual coal exhibit similar trends with varying extraction pressures, following the same pattern: at a constant temperature, the higher the pressure, the greater the CO_2 adsorption capacity. The adsorption capacity eventually stabilizes with changes in extraction pressure. The adsorption curves for raw and residual coal for each coal sample conform to Type I in the adsorption isotherm classification. Isothermal adsorption curves for anthracite before and after extraction at 8 MPa, 10 MPa, and 12 MPa are shown in Figure 7.

According to the adsorption fitting curve and data fitting results, both the BET and Langmuir models have high fitting coefficients for adsorption data, indicating that both models can be used to analyze the CO_2 adsorption process of coal when the experimental pressure is below 5 MPa. The fitting correlation coefficient of the Langmuir model is higher than that of the BET model, suggesting that the Langmuir model provides better fitting under the same conditions. In addition, the value of the saturated adsorption capacity (A) of each coal sample is larger than the adsorption capacity (V_m) of the first layer of CO_2 gas, and in the BET adsorption model, the number of adsorption layers (d) is also larger than 1, indicating that CO_2 gas molecules are adsorbed in multiple layers on the coal surface.

When analyzing the adsorption fitting curves of anthracite coal samples under different treatment conditions, it was found that the saturated adsorption capacity of residual coal after extraction by liquid CO_2 at different pressures was less than that of raw coal, with higher pressure resulting in a more significant reduction. The isothermal adsorption curves of residual coal from all coal samples were below that of raw coal, suggesting that oxygen-containing functional groups in coal were the potential adsorption sites. After liquid CO_2 extraction, small molecular organic compounds in coal pores dissolve out, causing a decrease in adsorption active sites and a reduction in micropore and mesopore proportions, as well as a decrease in the specific surface area of micropores. Consequently, the reaction area between the coal surface and CO_2 molecules is reduced, leading to a reduction in CO_2 adsorption capacity and the weakening of adsorption capacity. Under the same adsorption pressure (5 MPa), the adsorption capacity of raw coal was 34.23 cm^3/g, and after being extracted by liquid CO_2 at 8 MPa, 10 MPa, and 12 MPa, the adsorption capacity was 32.63 cm^3/g, 30.65 cm^3/g, and 28.47 cm^3/g, respectively.

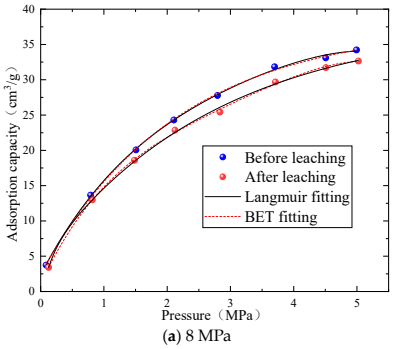

(**a**) 8 MPa

Figure 7. *Cont.*

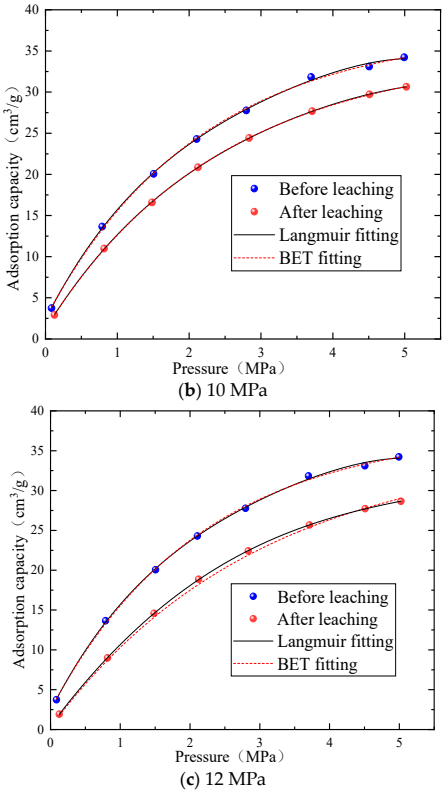

Figure 7. Isotherm adsorption curves of anthracite coal before and after leaching at 8 MPa, 10 MPa, and 12 MPa.

A coal seam is an anisotropic medium consisting of matrix pores and a natural fracture network, with its internal pore and fracture structure characteristics determining gas storage and migration. Following liquid CO_2 extraction, alterations in coal pore structure arise, subsequently affecting CO_2 adsorption properties within the coal. The evolution characteristics of specific surface area and adsorption capacity for bituminous coal before and after extraction at varying pressures are depicted in Figure 8.

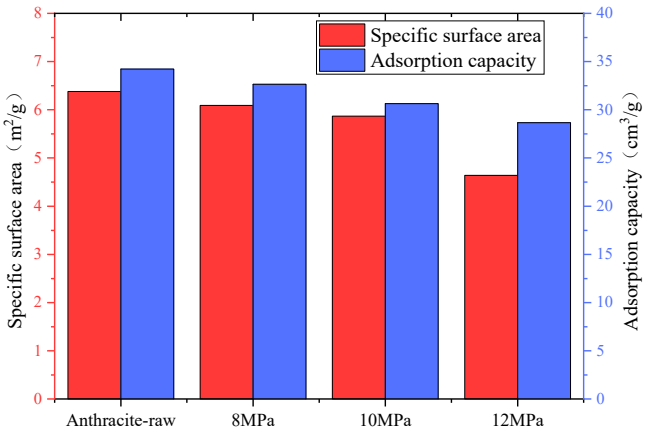

Figure 8. Evolution characteristics of specific surface area and adsorption capacity of bituminous coal before and after leaching under different pressures.

The coal's pore structure significantly influences its gas adsorption capacity, with the relationship between coal and gas adsorption closely associated with the coal micropores' specific surface area. Analyzing the specific surface area and adsorption capacity changes before and after extraction at different pressures reveals the raw coal's specific surface area and adsorption capacity to be 6.38 m^2/g and 34.23 cm^3/g, respectively. Following extraction

at 8 MPa, 10 MPa, and 12 MPa, the specific surface area was 6.09 m^2/g, 5.87 m^2/g, and 4.64 m^2/g, while the adsorption capacities were 32.57 cm^3/g and 30.66 cm^3/g, respectively.

Isothermal adsorption curves of bituminous coal before and after extraction at 8 MPa, 10 MPa, and 12 MPa are presented in Figure 9. The adsorption curve shape for raw coal and extracted residual coal aligns with curve I in the adsorption isotherm classification.

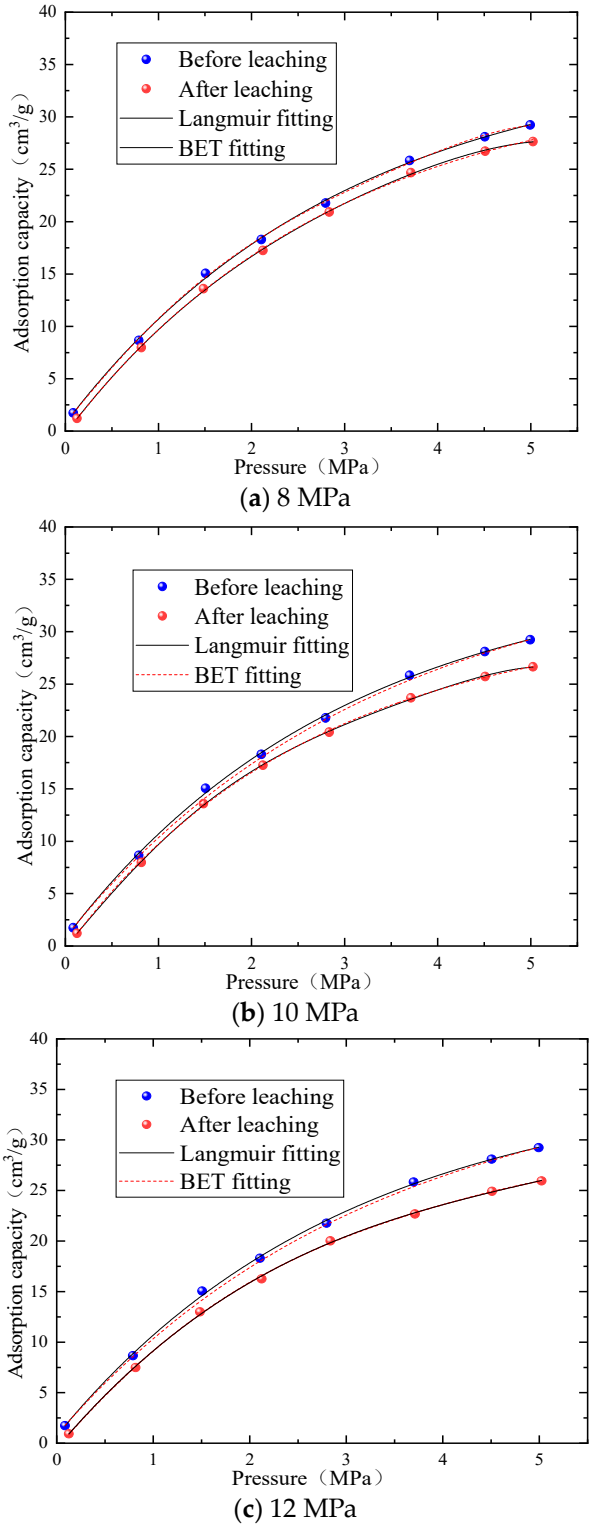

Figure 9. Isothermal adsorption curves of before and after leaching at 8 MPa, 10 MPa, and 12 MPa.

Considering the adsorption fitting curves and data fitting calculation results for bituminous coal under various pressures, both models can describe the CO_2 adsorption of bituminous coal. The residual coal's saturated adsorption capacity following liquid CO_2 extraction at different pressures was lower than that of raw coal, with the decline in adsorption capacity becoming more pronounced at higher pressures. At the same adsorption pressure (5 MPa), the raw coal's adsorption capacity was 29.23 cm^3/g, while the adsorption capacities were 27.65 cm^3/g, 26.52 cm^3/g, and 25.95 cm^3/g after extraction by liquid CO_2 at 8 MPa, 10 MPa, and 12 MPa, respectively. In the Langmuir model, the b value reflects the coal's low-pressure CO_2 adsorption rate, and a larger b value indicates a faster adsorption rate at low pressure. After extraction, the residual coal's b value was higher than that of raw coal, suggesting that residual coal has a higher low-pressure CO_2 adsorption rate than raw coal. When achieving the same adsorption capacity, the CO_2 gas pressure required for residual coal extraction was lower than that of raw coal, and the adsorption rate of residual coal was enhanced.

The evolution characteristics of specific surface area and adsorption capability for bituminous coal before and after various pressure extractions are presented in Figure 10. Following the dissolution of small and medium-sized organic molecules in coal, the pore structure of the extracted residual coal exhibits an expansion effect; simultaneously, the quantity of oxygen-containing functional groups, methyl and methylene groups, and aromatic ring functional groups on the surface decreases, which modifies the CO_2 adsorption sites in coal to a certain extent. By evaluating the variations in specific surface area and adsorption capability of bituminous coal before and after different pressure extractions, the specific surface area and adsorption capability of raw coal were determined to be 11.81 m^2/g and 29.23 cm^3/g, respectively. After 8 MPa, 10 MPa, and 12 MPa pressure extractions, the specific surface area was 9.67 m^2/g, 8.15 m^2/g, and 7.76 m^2/g, and the adsorption capability was 27.65 cm^3/g and 26 cm^3/g.

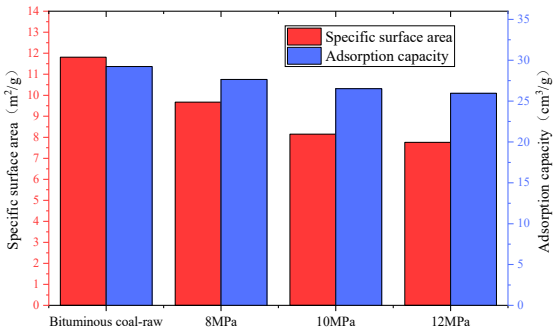

Figure 10. Evolution characteristics of specific surface area and adsorption capacity before and after leaching of anthracite under different pressures.

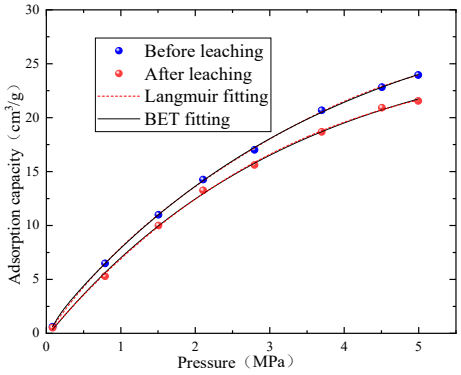

(**a**) 8 MPa

Figure 11. *Cont.*

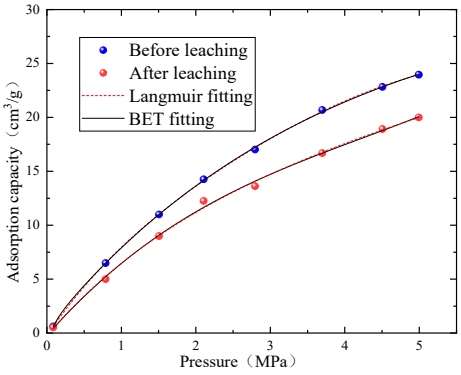

(**b**) 10 MPa

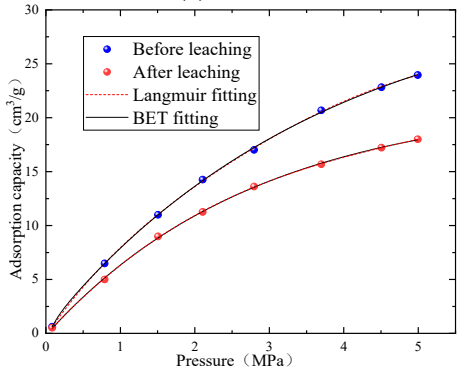

(**c**) 12 MPa

Figure 11. Isothermal adsorption curves of lignite before and after leaching at 8 MPa, 10 MPa, and 12 MPa.

The isothermal adsorption curves of lignite before and after extraction at 8 MPa, 10 MPa, and 12 MPa are displayed in Figure 11, conforming to the Type I curves in the adsorption isotherm classification.

Following liquid CO_2 extraction, the coal's pore structure undergoes changes, though its capacity to adsorb gas remains unaffected. Based on the adsorption fitting curve and data fitting computation table of lignite under various pressures, the saturated adsorption capability of residual coal extracted by liquid CO_2 under different pressures is lower than that of raw coal, and the adsorption capability decreases more prominently with increasing pressure. After liquid CO_2 extraction, the micro-molecule organic compounds in coal pores dissolve, resulting in a reduction in the number of micropores and CO_2 adsorption sites and weakening the adsorption capability. Under the same adsorption pressure (5 MPa), the adsorption capability of raw coal was 23.95 cm^3/g, while after extraction with liquid CO_2 at 8 MPa, 10 MPa, and 12 MPa, the adsorption capability was 21.56 cm^3/g, 20.01 cm^3/g, and 18.98 cm^3/g, respectively. The evolution characteristics of specific surface area and adsorption capability of lignite before and after various pressure extractions are shown in Figure 12.

By examining the variations in specific surface area and adsorption capability of lignite before and after different pressure extractions, the specific surface area and adsorption capability of raw coal were found to be 15.48 m^2/g and 23.95 cm^3/g, respectively. After 8 MPa, 10 MPa, and 12 MPa pressure extractions, the specific surface area was 15.03 m^2/g, 14.48 m^2/g, and 13.26 m^2/g, and the adsorption capability was 21.56 cm^3/g.

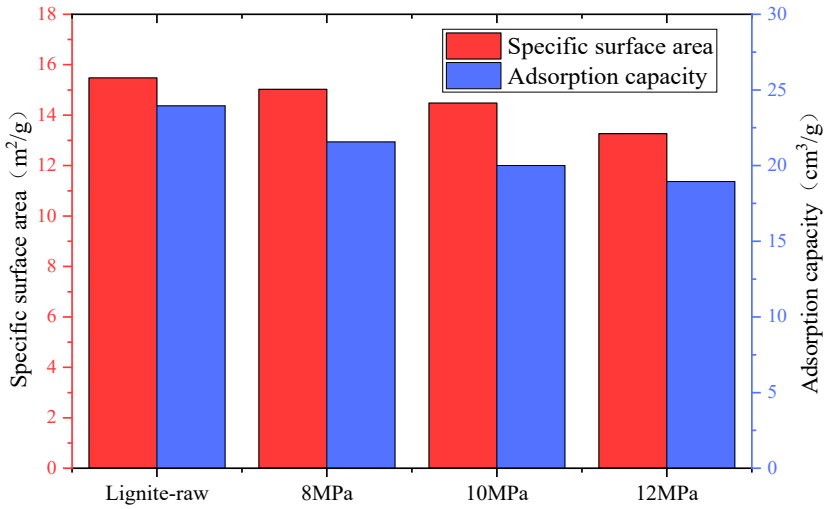

Figure 12. Evolution characteristics of specific surface area and adsorption capacity of lignite before and after leaching under different pressures.

4.2. CO_2 Adsorption Characteristics before and after Coal Dissolution

Isothermal adsorption profiles of anthracite pre- and post-dissolution at 1 MPa, 3 MPa, and 5 MPa are depicted in Figure 13, conforming to Type I curves in the adsorption isotherm classification.

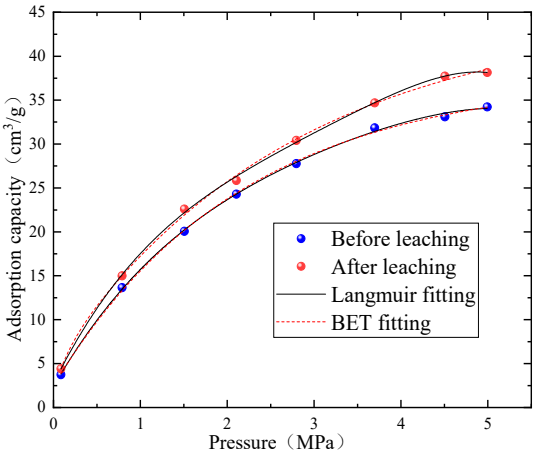

(**a**) 1 MPa

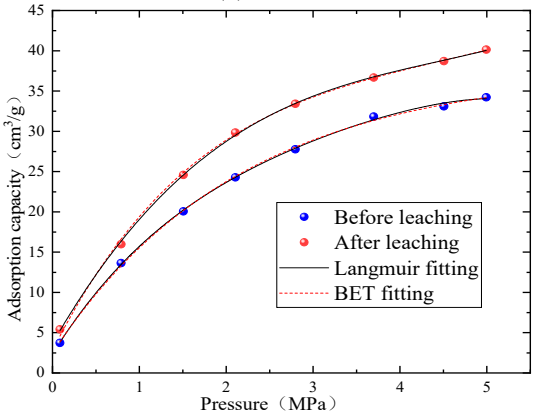

(**b**) 3 MPa

Figure 13. *Cont.*

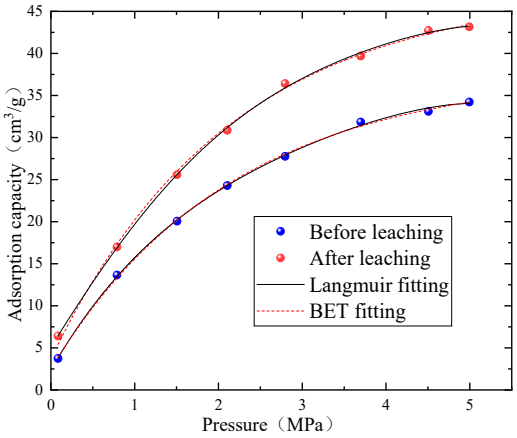

(**c**) 5 MPa

Figure 13. Isotherm adsorption curves of anthracite before and after dissolution at 1 MPa, 3 MPa and 5 MPa.

A coal seam consists of a porous medium with pores and fractures. The pore structure distribution governs the gas storage state and diffusion pattern in coal, whereas the fracture system distribution controls gas migration and mass transfer within the coal. The development characteristics and connectivity of pores and fissures are directly linked to CO_2 adsorption properties.

The adsorption capacity change law of anthracite before and after dissolution at various pressures is analogous to that of bituminous coal. Upon anthracite dissolution by 1 MPa, 3 MPa, and 5 MPa CO_2, the micropore count and specific surface area increased, and adsorption capacity incrementally rose with increasing dissolution pressure. The specific surface area and adsorption capacity changes of lignite pre- and post-dissolution at different pressures are illustrated in Figure 14.

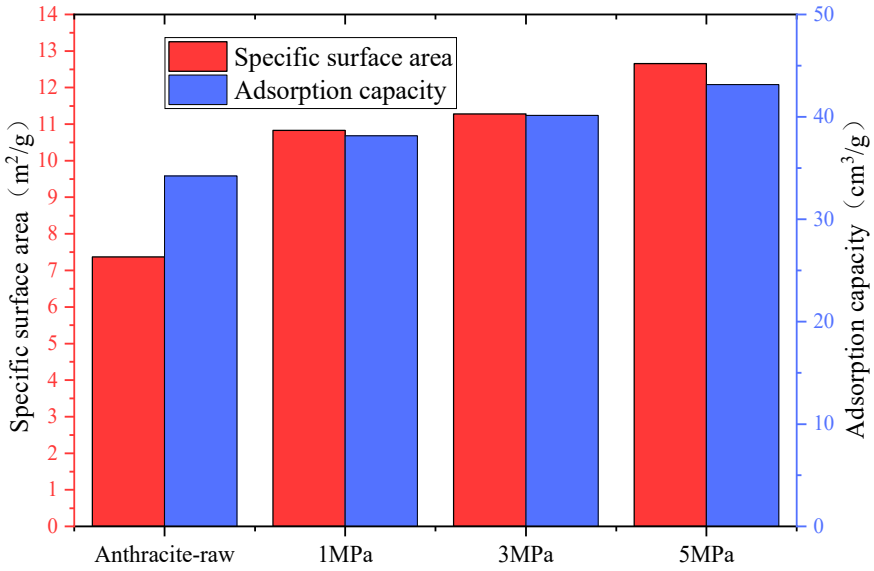

Figure 14. Evolution characteristics of specific surface area and adsorption capacity before and after leaching of anthracite at different pressures.

The raw coal's specific surface area and adsorption capacity were 7.37 m^2/g and 34.23 cm^3/g, respectively. Following corrosion at 1 MPa, 3 MPa, and 5 MPa, the residual coal's specific surface area was 10.83 m^2/g, 11.28 m^2/g, and 12.66 m^2/g, and the adsorption capacity was 38.56 cm^3/g, 40.15 cm^3/g, and 43.24 cm^3/g, respectively.

Figure 15 presents isothermal adsorption curves of bituminous coal pre- and post-corrosion at 1 MPa, 3 MPa, and 5 MPa. Following 1 MPa, 3 MPa, and 5 MPa CO_2 pressure corrosion, the adsorption capacity of the residual coal surpassed that of the raw coal, and the adsorption capacity progressively rose as corrosion pressure increased. The mineral dissolution process led to an augmentation in the quantity of micropores, transition pores, and mesopores, which proved advantageous for CO_2 gas adsorption.

Figure 16 illustrates the evolutionary traits of specific surface area and adsorption capacity of bituminous coal pre- and post-dissolution under different pressures. The specific surface area and adsorption capacity of raw coal were 7.37 m^2/g and 29.23 cm^3/g, respectively. After undergoing corrosion at 1 MPa, 3 MPa, and 5 MPa, the specific surface area of residual coal reached 10.83 m^2/g, 11.28 m^2/g, and 12.66 m^2/g, while the adsorption capacity measured 34.20 cm^3/g, 39.65 cm^3/g, and 42.14 cm^3/g, respectively.

The isothermal adsorption curves of lignite pre- and post-dissolution at 1 MPa, 3 MPa, and 5 MPa are displayed in Figure 17, with trends aligning with those of bituminous coal and anthracite coal. Following mineral dissolution, the adsorption capacity experienced an increase.

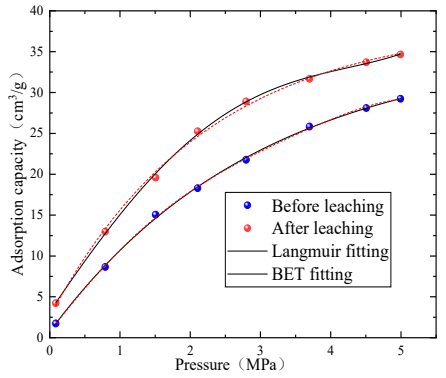

(**a**) 1 MPa

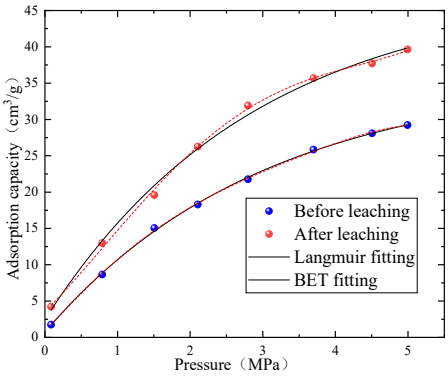

(**b**) 3 MPa

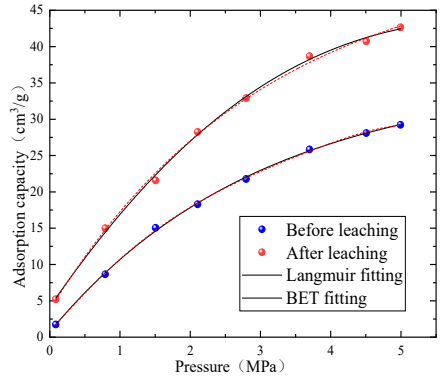

(**c**) 5 MPa

Figure 15. Isothermal adsorption curves of before and after dissolution at 1 MPa, 3 MPa, and 5 MPa.

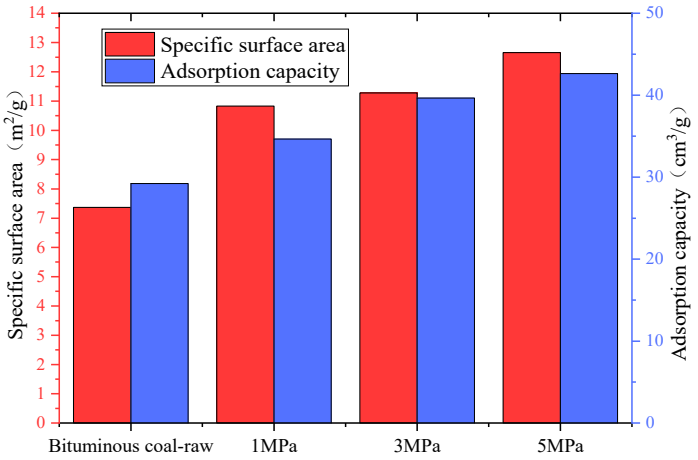

Figure 16. Evolution characteristics of specific surface area and adsorption capacity of bituminous coal before and after leaching under different pressures.

Adsorption capacity grows rapidly during low-pressure stages, while its upward trajectory is more gradual at high-pressure stages. Increased pore pressure is believed to heighten the impact frequency of gas molecules on the microscopic pore surface and the free-phase partial pressure, thereby disrupting the adsorption–desorption dynamic equilibrium and enhancing gas adsorption capacity. In low-pressure stages, a majority of adsorption sites within coal adsorption holes remain vacant, leading to rapid adsorption capacity growth. During high-pressure stages, adsorption sites are essentially saturated and gas molecules primarily fill micropores, causing the adsorption capacity to rise slowly until maximum adsorption capacity is attained. The raw coal's adsorption capacity was 23.95 cm^3/g under the same adsorption pressure (5 MPa) post-corrosion. Following 1 MPa, 3 MPa, and 5 MPa CO_2 corrosion, the adsorption capacities were 26.55 cm^3/g, 29.72 cm^3/g, and 32.45 cm^3/g, respectively. The evolutionary traits of specific surface area and adsorption capacity of lignite pre- and post-extraction under various pressures are shown in Figure 18.

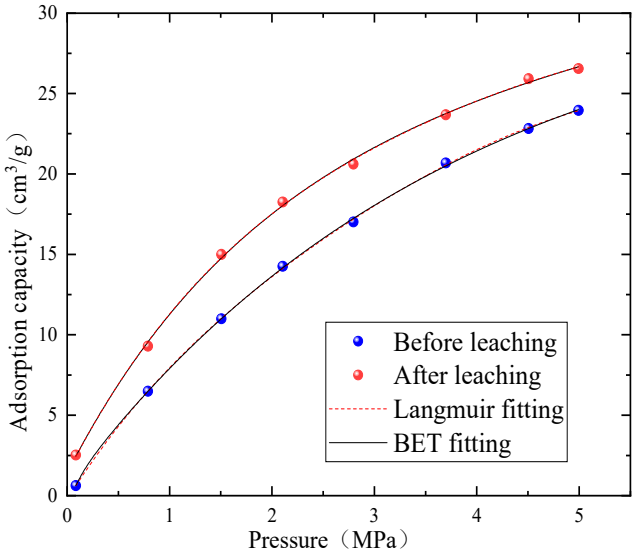

(**a**) 1 MPa

Figure 17. *Cont.*

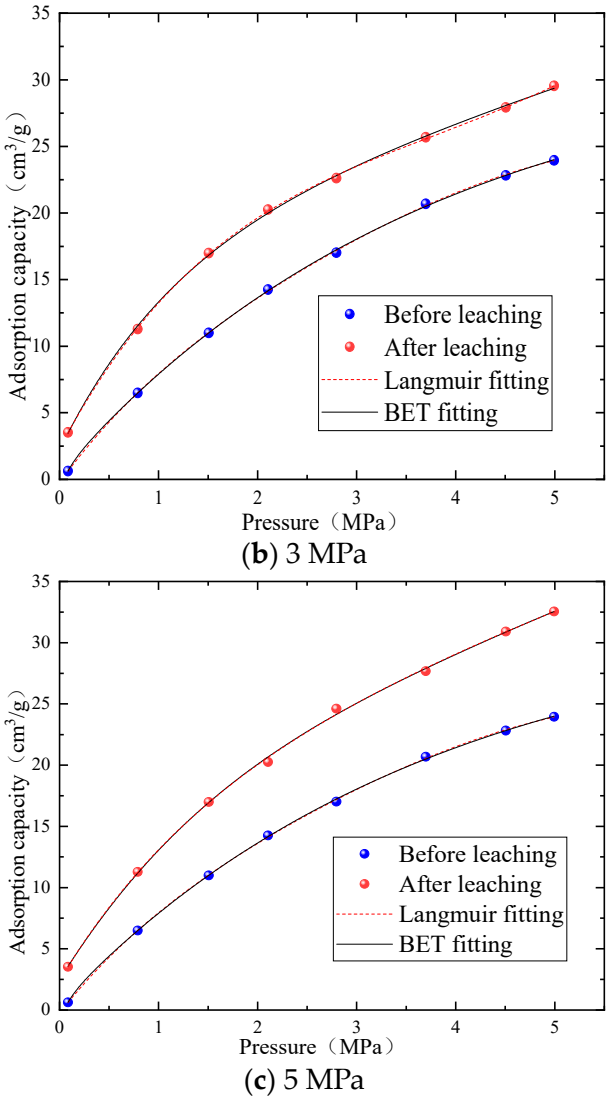

Figure 17. Isothermal adsorption curves of lignite before and after dissolution at 1 MPa, 3 MPa, and 5 MPa.

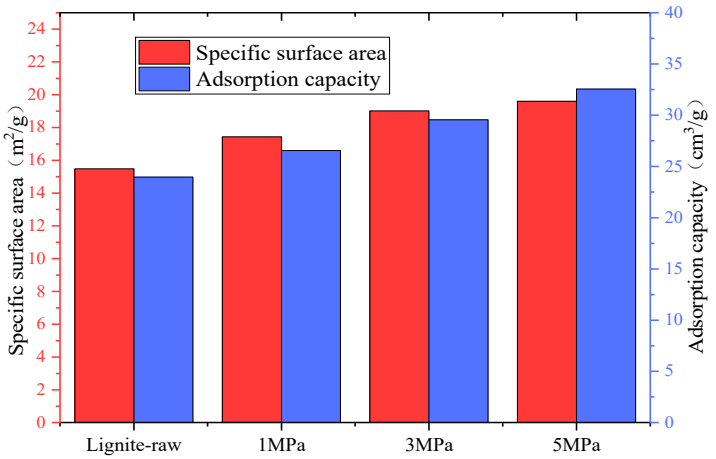

Figure 18. Evolution characteristics of specific surface area and adsorption capacity of lignite before and after leaching under different pressures.

The specific surface area and adsorption capacity of unprocessed coal were 15.48 m^2/g and 23.95 cm^3/g, respectively. After corrosion by 1 MPa, 3 MPa, and 5 MPa, the specific surface area and adsorption capacity of residual coal were 17.45 m^2/g, 19.01 m^2/g, 19.68 m^2/g, 26.51 cm^3/g, 29.47 cm^3/g, and 32.64 cm^3/g, respectively.

5. Discussion

Coal, a porous medium, is composed of pores and fissures. The distribution of coal's pore structure governs the storage state and diffusion mode of gas in coal, while the fissure system's distribution controls the migration and mass transfer movement of gas in coal [23–26]. The development characteristics and connectivity of pores and fissures are directly related to CO_2 adsorption properties.

Adsorption capacity increases rapidly in low-pressure stages, whereas the upward trend is more gradual in high-pressure stages. The rise in pore pressure enhances the impact frequency of gas molecules on the microscopic pore surface, disrupting the dynamic equilibrium between adsorption and desorption. In low-pressure stages, adsorption sites in coal's adsorption holes are mostly vacant, resulting in a rapid increase in adsorption capacity. In high-pressure stages, adsorption sites are nearly saturated, and gas molecules primarily occupy micropores. The adsorption capacity increases slowly until it reaches maximum capacity.

6. Conclusions

1. CO_2 gas molecule adsorption on coal surfaces exhibited multi-layer adsorption behavior. The saturated adsorption capacity of residual coal extracted by liquid CO_2 at different pressures was lower than that of raw coal. The higher the pressure, the more apparent this trend. Isothermal adsorption curves for residual coal from all samples were below those of raw coal.
2. Following liquid CO_2 extraction, small molecular organic compounds in coal pores dissolve, reducing adsorption-active sites. The proportion of micropores and mesopores in coal and the specific surface area of micropores decreased, resulting in a reduced reaction area between the coal surface and CO_2 molecules. Adsorption capacity decreased with the reduction in extraction pressure. After extraction of anthracite, bituminous coal, and lignite, the decrease in adsorption capacity diminished sequentially.
3. After anthracite, bituminous coal, and lignite underwent corrosion by 1 MPa, 3 MPa, and 5 MPa CO_2, the number of micropores increased, the specific surface area rose, and the adsorption capacity gradually increased with the corrosion pressure. The average adsorption increment for anthracite, bituminous coal, and lignite was 9.01 cm^3/g, 12.91 cm^3/g, and 8.69 cm^3/g, respectively. The adsorption increment for bituminous coal was greater than that for anthracite and lignite. Following corrosion, bituminous coal was more suitable for CO_2 geological storage.

Author Contributions: H.W. (Hu Wen) is the project administer. H.W. (Hu Wang) wrote the original draft. Z.L. conducted an investigation. W.M. conducted experiments. All authors have read and agreed to the published version of the manuscript.

Funding: This work was supported by the National Natural Science Foundation of China (Grant No. 51804245 and 51504186) and National Key R&D Projects (Programs 2016YFC0801802 and 2018YFC0808201).

Conflicts of Interest: The authors declare that they have no known competing financial interests or personal relationships that could have appeared to influence the work reported in this paper.

Nomenclature

θ	The adsorption mass coverage, %	S_θ	The surface area of the solid covered by adsorbate, m^2
S_t	The total surface area of the solid, m^2	N	The number of collision molecules per unit surface area per unit time
P	The gas pressure, MPa	m	The molecular mass of gas, g
k	Boltzman constant	T	The absolute temperature, K.
V_a, V_d	Adsorption rates and desorption rates, cm^3/s	α	The fraction adsorbed in the collision molecule A
v	The desorption proportional constant	a, b	Adsorption equilibrium constants
P_0	Saturated vapor pressure of adsorbate at a fixed temperature, MPa	C	Adsorption process constant
V_m	The saturated adsorption capacity of the first layer, cm^3/g temperature, MPa	d	Fixed constant, which is related to Temperature, pore distribution, etc.
V	The gas volume, cm^3	n	The amount of substance, mol
Z	The gas compression factor dimensionless	R	The gas constant, 8.314 J/(mol·K)

References

1. Yuan, L. Control of coal and gas outbursts in Huainan mines in China: A review. *J. Rock Mech. Geotech. Eng.* **2016**, *8*, 559–567. [CrossRef]
2. Liu, P.; Nie, B.; Zhao, Z.; Zhao, Y.; Li, Q. Characterization of ultrasonic induced damage on multi-scale pore/fracture in coal using gas sorption and μ-CT 3D reconstruction. *Fuel* **2023**, *332*, 126178. [CrossRef]
3. Chen, X.; Li, L.; Wang, L.; Qi, L. The current situation and prevention and control countermeasures for typical dynamic disasters in kilometer-deep mines in China. *Saf. Sci.* **2019**, *115*, 229–236. [CrossRef]
4. Liu, P.; Fan, L.; Fan, J.; Zhong, F. Effect of water content on the induced alteration of pore morphology and gas sorption/diffusion kinetics in coal with ultrasound treatment. *Fuel* **2021**, *306*, 121752. [CrossRef]
5. Wu, J.; Yu, J.; Wang, Z.; Fu, X.; Su, W. Experimental investigation on spontaneous imbibition of water in coal: Implications for methane desorption and diffusion. *Fuel* **2018**, *231*, 427–437. [CrossRef]
6. Wen, H.; Wang, H.; Fan, S.; Li, Z.; Chen, J.; Cheng, X.; Cheng, B.; Yu, Z. Improving coal seam permeability and displacing methane by injecting liquid CO_2: An experimental study. *Fuel* **2020**, *281*, 118747. [CrossRef]
7. Guo, H.; Cheng, Y.; Wang, L.; Lu, S.; Jin, K. Experimental study on the effect of moisture on low-rank coal adsorption characteristics. *J. Nat. Gas Sci. Eng.* **2015**, *24*, 245–251. [CrossRef]
8. Liu, Z.; Cheng, Y.; Wang, Y.; Wang, L.; Li, W. Experimental investigation of CO_2 injection into coal seam reservoir at in-situ stress conditions for enhanced coalbed methane recovery. *Fuel* **2019**, *236*, 709–716. [CrossRef]
9. Zhang, R.; Cheng, Y.; Yuan, L.; Zhou, H.; Wang, L.; Zhao, W. Enhancement of gas drainage efficiency in a special thick coal seam through hydraulic flushing. *Int. J. Rock Mech. Min. Sci.* **2019**, *124*, 104085. [CrossRef]
10. Liu, P.; Fan, L.; Li, Q.; Zhong, F. Power ultrasound assisted coalbed methane enhancement recovery: Field application and performance evaluation in underground coal mine. *Fuel* **2022**, *324*, 124575. [CrossRef]
11. Fortin, J.; Schubnel, A.; Guéguen, Y. Elastic wave velocities and permeability evolution during compaction of Bleurswiller sandstone. *Int. J. Rock Mech. Min. Sci.* **2005**, *42*, 873–889. [CrossRef]
12. Wang, S.; Elsworth, D.; Liu, J. Permeability evolution during progressive deformation of intact coal and implications for instability in underground coal seams. *Int. J. Rock Mech. Min. Sci.* **2013**, *58*, 34–45. [CrossRef]
13. Wang, L.; Liu, S.; Cheng, Y.; Yin, G.; Zhang, D.; Guo, P. Reservoir reconstruction technologies for coalbed methane recovery in deep and multiple seams. *Int. J. Min. Sci. Technol.* **2017**, *27*, 277–284. [CrossRef]
14. Liu, P.; Liu, A.; Liu, S.; Qi, L. Experimental evaluation of ultrasound treatment induced pore structure and gas desorption behavior alterations of coal. *Fuel* **2021**, *307*, 121855. [CrossRef]
15. Liu, P.; Nie, B.; Zhao, Z.; Li, J.; Yang, H.; Qin, C. Permeability of micro-scale structure in coal: Insights from μ-CT image and pore network modelling. *Gas Sci. Eng.* **2023**, *111*, 204931. [CrossRef]
16. Liu, P.; Liu, A.; Zhong, F.; Jiang, Y.; Li, J. Pore/fracture structure and gas permeability alterations induced by ultrasound treatment in coal and its application to enhanced coalbed methane recovery. *J. Pet. Sci. Eng.* **2021**, *205*, 108862. [CrossRef]
17. Krooss, B.M.; Gensterblum, Y.; Siemons, N.; Van Bergen, F.; Pagnier, H.J.M.; David, P. High-pressure methane and carbon dioxide adsorption on dry and moisture-equilibrated Pennsylvanian coals. *Int. J. Coal Geol.* **2002**, *51*, 69–92. [CrossRef]
18. Stevens, S.H.; Kuuskraa, V.A.; Gale, J.; Beecy, D. CO_2 injection and sequestration in depleted oil and gas fields and deep coal seams: Worldwide potential and costs. *Environ. Geosci.* **2001**, *8*, 200–209. [CrossRef]
19. Abunowara, M.; Bustam, M.A.; Sufian, S.; Babar, M.; Eldemerdash, U.; Mukhtar, A.; Ullah, S.; Assiri, M.A.; Al-Sehemi, A.G.; Lam, S.S. High pressure CO_2 adsorption onto Malaysian Mukah-Balingian coals: Adsorption isotherms, thermodynamic and kinetic investigations. *Environ. Res.* **2023**, *218*, 114905. [CrossRef]
20. Shang, Z.; Wang, H.; Li, B.; Cheng, Y.; Zhang, X.; Wang, Z.; Geng, S.; Wang, Z.; Chen, P.; Lv, P.; et al. The effect of leakage characteristics of liquid CO_2 phase transition on fracturing coal seam: Applications for enhancing coalbed methane recovery. *Fuel* **2022**, *308*, 122044. [CrossRef]

21. Li, Z.; Wang, F.; Shu, C.M.; Wen, H.; Wei, G.; Liang, R. Damage effects on coal mechanical properties and micro-scale structures during liquid CO_2-ECBM process. *J. Nat. Gas Sci. Eng.* **2020**, *83*, 103579. [CrossRef]
22. Zhai, X.; Ge, H.; Obracaj, D. The cooling range of liquid CO_2 on loose coal through experimental investigation. *Int. J. Oil Gas Coal Technol.* **2021**, *27*, 54–77. [CrossRef]
23. Zhang, L.; Wang, Y.; Liu, M.; Wang, L.; Liu, H. Multiple-flow-regime models for real gas transport in fractal porous media at high pressure. *J. Pet. Sci. Eng.* **2021**, *196*, 107684. [CrossRef]
24. Liu, J.; Chen, Z.; Elsworth, D.; Qu, H.; Chen, D. Interactions of multiple processes during CBM extraction: A critical review. *Int. J. Coal Geol.* **2011**, *87*, 175–189. [CrossRef]
25. Liu, H.H.; Rutqvist, J. A new coal-permeability model, internal swelling stress and fracture–matrix interaction. *Transp. Porous Media* **2010**, *82*, 157–171. [CrossRef]
26. Valliappan, S.; Wohua, Z. Numerical modelling of methane gas migration in dry coal seams. *Int. J. Numer. Anal. Methods Geomech.* **2015**, *20*, 571–593. [CrossRef]